GEM TN-91-32

Signal and Background of $H \rightarrow \gamma\gamma$ with Proposed GEM Calorimeter Systems

November 30, 1991

Abstract:

This report summarizes main results of a study on signal and background for $H \rightarrow \gamma\gamma$ detection at SSC by using two precision electromagnetic calorimeter options (BaF_2 and liquid argon) proposed by GEM collaboration. The consequence of thermal as well as pile-up noise in isolation cone is discussed. A brief discussion of intermediate mass Higgs detection by using associated production channel $Htt \rightarrow \ell\gamma\gamma$ is also given.

Signal and Background of H$\rightarrow \gamma\gamma$ with Proposed GEM Calorimeter Systems

Ren-yuan Zhu[1]

Lauritsen Laboratory
California Institute of Technology
Pasadena, CA 91125

November 30, 1991

Abstract

This report summarizes main results of a study on signal and background for H$\rightarrow \gamma\gamma$ detection at SSC by using two precision electromagnetic calorimeter options (BaF_2 and liquid argon) proposed by GEM collaboration. The consequence of thermal as well as pile-up noise in isolation cone is discussed. A brief discussion of intermediate mass Higgs detection by using associate production channel $Ht\bar{t} \rightarrow \ell\gamma\gamma$ is also given.

1 Introduction

As a precision lepton photon detector, the discovery potential of the GEM (Gamma-Electron-Muon) detector is shown in its ability to detect Higgs particles in a mass range between 80 and 180 GeV through its $\gamma\gamma$ and 4ℓ (ZZ^*) modes [1]. While the 4ℓ decay mode will allow GEM to detect a Higgs with a mass heavier than 140 GeV, the $\gamma\gamma$ decay mode will cover a gap between the upper limit for Higgs detection at LEP Phase II (80 GeV) [2] and 140 GeV.

H$\rightarrow \gamma\gamma$ detection places strigent requirements on the overall detector design, especially on the design of the electromagnetic calorimeter (EMC). Because of the small production cross-section (50 to 200 fb) and the narrow decay width (5 to 10 MeV) of the Higgs boson in this mass range, and because of the huge irreducible direct

[1]Work supported in part by U.S. Department of Energy Contract No.DE-AC03-81-ER40050.

$\gamma\gamma$ background (276 pb) and the QCD jet background, precision EMCs, capable of measuring $\gamma\gamma$ invariant mass to a high precision, are pursued by GEM. Two options were proposed: a barium fluoride (BaF_2) crystal calorimeter and a liquid argon (LAr) accordion calorimeter.

This note reports a study on signal and background in Higgs searches by using $H \rightarrow \gamma\gamma$ channel for BaF_2 and LAr calorimeters. A brief discussion of intermediate mass Higgs detection by using associate production channel $Ht\bar{t} \rightarrow \ell\gamma\gamma X$ is also given.

The detector response for isolated photons was simulated according parametrized energy, position and vertex z resolutions:[2]

- **Energy Resolution:** $(2.0/\sqrt{E} \oplus 0.5)\%$ for BaF_2 and $(7.5/\sqrt{E} \oplus 0.5)\%$ for LAr;
- **Position Resolution:** $\delta x = \delta y = 1$ mm at front surface of EMC are used for both calorimeters;
- **Vertex z Resolution:** $\delta z = 0.5$ mm are used for both calorimeters. Photon momentum vector is reconstructed by using primary vertex position and its impact point at front surface of EMC.

Note, the acceptance loss because of dead space in detector was not included in this study. A more detailed study including consequences of dead space will be carried out for GEM technical report when detector design is more mature.

The Monte Carlo program used in this study is PYTHIA 5.5 [3], and the top quark mass is assumed to be 140 GeV. An SSC year (SSCY) is defined as 10^{40} cm^2 integrated luminosity.

2 Signal and Irreducible $\gamma\gamma$ Background

Figure 1 shows the production cross-sections of standard model Higgs in three interesting decay modes: a) $\gamma\gamma$, b) $Ht\bar{t} \rightarrow \ell\gamma\gamma$, and c) $ZZ^*/ZZ \rightarrow e^+e^-e^+e^-$, before event selection cuts.

For the Higgs mass range discussed in this report (80 to 150 GeV), the $\gamma\gamma$ decay mode provides 1200 to 2200 events per SSC year, while $Ht\bar{t} \rightarrow \gamma\gamma X$ provides 50 to 170 events per SSC year without lepton tagging, or 20 to 70 events with electron or muon

[2]The primary event vertex is assumed to be determined by using central tracker.

tagging. Table 1 lists production cross-section and number of events accepted after passing event selection cuts described in this report.

Table 1: Production Cross-Section and Events/SSCY

M_H(GeV)	$\sigma_{H(\gamma\gamma)}(fb)$	$N_{\gamma\gamma}$	$\sigma_{t\bar{t}H(\gamma\gamma)}$ (fb)	$N_{l\gamma\gamma}$	$\sigma_{H(4e)}(fb)$	N_{4e}
80	124	510	18	14		
90	144	620	17	16		
100	169	730	16	16		
120	211	960	14.5	14		
140	180	880	8.5	10	5.6	24
150	128	640	5.2	5	7.4	33
160	52.6	270	1.6	3	3.2	13
170					2.2	9
180					5.6	28
200					21.2	99
400					14.0	85
600					3.9	26
800					1.5	10

The main background in $H^0 \rightarrow \gamma\gamma$ searches is direct photon production [4]. The cross-section of this background was calculated to be 276 pb for $\hat{p}_T > 20$ GeV:

- $q\bar{q} \rightarrow \gamma\gamma$: 78 pb; and
- $gg \rightarrow \gamma\gamma$ via a box diagram: 198 pb.

The event topology of $H \rightarrow \gamma\gamma$ and this background are similar. Figure 2 shows transverse energy distributions in EMC for two typical events from signal process of $H \rightarrow \gamma\gamma$ signal (a) and $\gamma\gamma$ background (b). This so-called *"irreduciable background"* therefore has to be reduced by event selection cuts. Figure 3 shows the distributions of photon rapidity (η_γ), photon transverse energy (E_T^γ), rapidity of the 2 photon system ($\eta_{\gamma\gamma}$) and $\cos\theta^*$, where θ^* is the polar angle of photons in the $\gamma\gamma$ rest frame, for $H^0 \rightarrow \gamma\gamma$, $q\bar{q} \rightarrow \gamma\gamma$ and $gg \rightarrow \gamma\gamma$.

Event selection cuts used to reduce this background are:

- $|\eta_\gamma| < 2.5$;

- $E_T > 20$ GeV;
- $| cos\theta^*_\gamma | < 0.9 \Rightarrow$ reduce gg $\rightarrow \gamma\gamma$;
- $| \eta_{\gamma\gamma} | < 3 \Rightarrow$ reduce qq $\rightarrow \gamma\gamma$.

After event selection cuts, the cross-section of irreducible background is reduced to 42 pb for $M_{\gamma\gamma} > 75$ GeV, while the acceptance of H$\rightarrow \gamma\gamma$ events is more than 50%. Figure 4a) shows $\gamma\gamma$ invariant mass spectra collected in one SSCY with Higgs signals (80, 100, 120 and 150 GeV) superimposed over the irreduciable background for three energy resolutions: a) $(2/\sqrt{E} \oplus 0.5)\%$; b) $(7.5/\sqrt{E} \oplus 0.5)\%$; and c) $(15/\sqrt{E} \oplus 1)\%$. Corresponding background subtracted spectra are shown in d), e) and f).

The significance of these peaks can be calculated by dividing the number of signal events counted within $M_H \pm \sigma_{M_{\gamma\gamma}}$ by the square root of background events in the same mass interval, where $\sigma_{M_{\gamma\gamma}}$ is the $\gamma\gamma$ invariant mass resolution. As described above, this mass resolution was calculated taking into account the effects of energy resolution assumed, 1 mm position resolution at the front surface of EMC and 0.5 mm vertex z resolution.

Table 2 summarizes production cross-section and number of signal events (N_S) in $M_H \pm \sigma_{M_{\gamma\gamma}}$ for different Higgs masses. Also listed in the table are mass resolutions ($\sigma_{M_{\gamma\gamma}}$) and significances for three nominal energy resolutions.

Table 2: Significance of H$\rightarrow \gamma\gamma$ searches in one SSCY

$\Delta E/E$ (%)			$2/\sqrt{E} \oplus 0.5$		$7.5/\sqrt{E} \oplus 0.5$		$15/\sqrt{E} \oplus 1.0$	
M_H (GeV)	$\sigma_{\gamma\gamma}$ (fb)	N_S	$\sigma_{M_{\gamma\gamma}}$ (GeV)	$S/\sqrt{N_B}$	$\sigma_{M_{\gamma\gamma}}$ (GeV)	$S/\sqrt{N_B}$	$\sigma_{M_{\gamma\gamma}}$ (GeV)	$S/\sqrt{N_B}$
80	124	360	0.34	4.6	0.66	3.2	1.3	2.3
90	144	430	0.37	6.1	0.70	4.5	1.4	3.2
100	169	510	0.40	8.6	0.73	6.3	1.45	4.5
120	211	670	0.45	14	0.77	11	1.5	7.7
140	180	620	0.53	16	0.89	12	1.7	8.9
150	128	450	0.58	13	0.95	10	1.9	7.3
160	52.6	190	0.65	5.9	1.1	4.7	2.0	3.4

Table 2 shows clearly the importance of excellent energy resolution in pursuing this physics. In summary, there is a factor of $\sqrt{1.8}$ difference in significances of H$\rightarrow \gamma\gamma$

detection, or a factor of 1.8 difference in time needed to achieve certain significance, between two neighboring energy resolutions in above table.

To study systematically the effect of energy resolution, we parametrize the energy resolution of an EMC as a function of parameters **a** and **b**:

$$\frac{\Delta E}{E} = (\frac{\mathbf{a}}{\sqrt{\mathbf{E}}} \oplus \mathbf{b})\% \tag{1}$$

The result of this analysis, listed in Table 3, shows the time factors needed to discover a narrow $\gamma\gamma$ resonance as a function of **a** and **b**. To facilitate comparison the numbers in this table are normalized to the BaF_2 crystal calorimeter resolution: $2\%/\sqrt{E} \oplus 0.5\%$.

Table 3: Time factor in discovering a $\gamma\gamma$ resonance as functions of **a** and **b**

a	2.0	3.0	5.0	7.5	10	15
b=0	0.48	0.68	1.1	1.6	2.2	3.3
b=.25	0.63	0.83	1.2	1.7	2.2	3.3
b=0.5	1.0	1.1	1.4	1.8	2.3	3.4
b=.75	1.4	1.5	1.7	2.1	2.6	3.6
b=1.0	1.8	1.9	2.1	2.4	2.9	3.7

It is also interesting to see the effect of shower position resolution. Table 4 shows the time factors needed to discover a narrow $\gamma\gamma$ resonance as a function of the shower position resolution, δx and **a**, assuming **b** = 0.5. The numbers in this table are also normalized to the BaF_2 crystal calorimeter resolutions: **a** = 2 and $\delta x = \delta y = 1$ mm.

Table 4: Time factor in discovering a $\gamma\gamma$ resonance as function of δx and **a**, for **b**=0.5

δx(mm)	0.5	1.0	1.5	2.0	3.0	5.0
a=1	0.94	0.95	0.97	1.0	1.1	1.4
a=2	1.0	1.0	1.0	1.1	1.2	1.4
a=3	1.1	1.1	1.1	1.2	1.3	1.5
a=5	1.4	1.4	1.4	1.4	1.5	1.7
a=7.5	1.8	1.8	1.8	1.9	1.9	2.1

To be complete, Table 5 shows the effect of vertex z resolution in discovering a narrow $\gamma\gamma$ resonance as functions of the vertex z coordinate resolution (δz), **a** and **b**, assuming shower position resolution $\delta x = 1$ mm. The numbers in this table are normalized to the BaF_2 crystal calorimeter resolutions: **a** = 2 and **b** = 0.5. It is clear one must determine vertex z to about mm level, so that the discovery potential of a high energy resolution EMC is not compromised.

Table 5: Time factor in discovering a $\gamma\gamma$ resonance as function of δz, **a** and **b**

a	**b**	δz=0.5 mm	δz=10 mm	δz=50 mm
2	0.5	1	1.6	5.0
7.5	0.5	1.9	2.3	5.2
15	1	3.8	4.0	6.1

3 QCD Jets Background

If there were no other background, the analysis for H$\rightarrow \gamma\gamma$ searches would have been finished in section 2. However, there are copious π^0's, and thus photons, produced in QCD jets. There are two major background from QCD jets: γ-jet and 2 jets final states. The production cross-section of γ-jet is 237 nb for $\hat{p}_T > 20$ GeV, including the following processes:

- $qg \rightarrow \gamma q$: 226 nb; and
- $qq \rightarrow \gamma g$: 11 nb.

The production cross section of QCD 2jets is 2 mb for $\hat{p}_T > 20$ GeV, including the following final states:

- gg: 1.54 mb;
- gq: 0.44 mb; and
- qq: 0.043 mb.

A narrow neutral jet consisting of multiple photons would fake an isolated photon. Single photons may also be produced in parton shower process. Figure 5 shows transverse energy distributions in EMC for two typical events from background processes: (a) γ-jet and (b) 2jets. To identify real photon and to reject QCD jet background, isolation cuts, shower shape analysis and preradiator may be used. The huge cross-section of these background processes make an accurate GEANT simulation not feasible in near future with foreseen computer power. It is thus crucial to use GEANT based parametrization to obtain a realistic estimation of the background cross-section. In this section, the result of jet rejection cuts is presented in terms of QCD jet background cross-section in a mass range between 75 to 165 GeV.

It is interesting to note that at "parton" level[3] distributions of the invariant mass of $\gamma\gamma$, γ-jet and 2jets are similar at high mass end, as shown in Figure 6. After implementing the isolation cut described below, the energy vector of a fake isolated photon, in general, follows that of its parent parton. It is thus reasonable to assume that the $\gamma\gamma$ spectra from all three background processes have similar shape. Therefore, we need only to calculate γ/jet rejection ratio for a given rejection cut, and to deduce corresponding background cross-section for a given background process.

We further use relevant integrated cross-section, e.g. in a mass range between 75 and 165 GeV, to calculate total background cross-sections, and find significances for a given Higgs signal by scaling. Note, the shower shape and preradiator cuts described in this report do not change cross-sections of the Higgs signal and the irreducible $\gamma\gamma$ background very much, since the efficiency for single isolated photon passing these cuts are required to be larger than 90%.

3.1 Parametrized Response of Calorimeters

For background calculation, a parametrized response of calorimeters was used in this analysis. The calorimeter was defined in $|\eta| < 2.5$, and was segmented to $\Delta\eta \times \Delta\phi = 0.04 \times 0.04$ in both EMC and hadron calorimeter (HCAL) sections. No longitudinal segmentation in EMC or HCAL was assumed.

The longitudinal energy division between EMC and HCAL was assigned based upon a GEANT study for BaF_2 calorimeter [5]. All γ/electrons have 100% of their energies deposited in EMC. All muons are minimum ionizing, i.e. deposit minimum ionizing energy (MIE) in EMC. For charged hadrons, if its energy is less than 2 MIE

[3]We denote photon as one of the partons together with quarks and gluons.

then all its energy were deposited in EMC, otherwise it has 25% probability of depositing MIE in EMC, and 75% probability of depositing a fraction of its energy in EMC with the rest in HCAL. This fraction was determined according to a uniform distribution between MIE and about 80% of the energy of the hadron.

The energies deposited in EMC and HCAL were further divided to 50 pieces and deposited to cells according to lateral shower profile. This process provides a first order approximation of energy distribution in EMC/HCAL cells, and was also used in trigger rate study [5].

3.2 Isolation Cut

The isolation cut uses the following procedure:

- Generate γ-jet or 2jets, use only jets within detector acceptance and with $E_T >$ 20 GeV. Deposit energies of complete events in calorimeter cells, as described in section 3.1. Mark cells which were hit by charged track in 8 kG field.
- Search through all cells to identify those cells hit by photons only, find E_T^{cell}.
- Charge Veto:

  Search through neighboring 8 cells, if any cell is hitted by a charged track or its E_T^{cell} is larger than that of the central cell $\Rightarrow$ **Reject**;
- Define the sum of E_T^{cell}'s of these 9 cells ($\sum_{9cells} E_T^{cell}$) as the E_T^{photon};
- Isolation Veto:

  if the sum of the transverse energies in a cone of radius R ($R=\sqrt{\Delta\eta^2 + \Delta\phi^2}$), excluding the E_T^{photon}, is larger than 10% of the E_T^{photon} plus an isolation energy cut (E_T^{cut}):

$$\sum_{r<R} E_T - E_T^{photon} > (E_T^{cut} + 0.1 E_T^{photon}) \Rightarrow \textbf{Reject}. \qquad (2)$$

Table 6 shows the result of γ/jet isolation rejection ratios as function of the size of isolation cone (R) and the E_T^{cut}, for two QCD processes.

It is interesting to note that the rejection ratios from γ-jet and 2jets processes are different. This can be explained by different jet composition of these two processes.

Table 6: Rejection Ratio (10^{-4})

Process	2jets			γ-jet		
E_T^{cut}	R=0.45	R=0.60	R=0.75	R=0.45	R=0.60	R=0.75
5 GeV	5.3	4.1	3.1	16	13	9.6
10 GeV	8.8	6.8	6.2	30	26	22
15 GeV	13	10	8.6	40	34	32
20 GeV	16	14	13	54	47	43

Since QCD 2jets have 12% quark jets and 88% gluon jets, while γ-jet have 95% quark jets and 5% gluon jets, we deduce that the isolation rejection ratio is about 10^{-3} for the quark jet and 2×10^{-4} for the gluon jet when the tightest isolation cut is used, i.e. 5 GeV E_T^{cut} in a 0.75 cone. We further attribute this factor of 5 difference in isolation rejection to:

- gluon jet is more broader than the quark jet in fragmentation; and
- gluon jet has lower probability of emitting a hard photon than a quark jet.

3.3 Further Rejection of Isolated Photon Candidate

The isolation cut along can not reduce the QCD jets background to below irreducible $\gamma\gamma$ background level. Looking at the isolated photon candidate (IPC) in details, however, one finds that many IPCs consist of more than one photons, and thus can be rejected by using shower shape analysis or preradiator. Figure 7 shows distributions of number of photons in isolated photon candidates after an isolation cut of R = 0.75 and E_T^{cut} = 10 GeV for 100k events each of a) γ-jet and b) 2jets events.

A calculation was carried out to select IPCs passing a rough isolation cut: R = 0.45 and E_T^{cut} = 20 GeV. Events samples with one IPC from 2jets process and two IPCs from γ-jet process were recorded in data files on physics detector simulation facility (PDSF) disk at SSCL for further analysis.

To identify how close the IPCs are to a real photon, an energy weighted mean opening angle, $\bar{\theta}$, is calculated for each IPC:

$$\bar{\theta} = \frac{\sum_i E_i \theta_i}{\sum_i E_i} \tag{3}$$

where

$$\cos\theta_i = \frac{\vec{E}_i \cdot \vec{n}}{E_i}, \quad \vec{n} = \frac{\sum_i \vec{E}_i}{|\sum_i \vec{E}_i|}, \tag{4}$$

and $\vec{E}_i$ is the energy vector of the ith photon in the isolated photon candidate.

Figure 8 shows $\bar{\theta}$ distributions of isolated photon candidates after an isolation cut of R = 0.75 and E_T^{cut} = 10 GeV obtained from 100k events each of a) γ-jet and b) 2jets events. It is clear that those ICPs with a large $\bar{\theta}$ may be rejected by using shower shape analysis.

A detailed GEANT study by H. Yamamoto shows that in average, ICPs with $\bar{\theta} > 5$ mrad may be rejected by using a shower shape cut [6]. His analysis is based upon a fit on lateral shower profile in BaF_2 to an oval Gaussian distribution, and reject those ICPs with large minor. The simulation includes a rotation of all particles in IPCs, making $\vec{n}$ aiming randomly at the full area of the central crystal. The vertex z position, where ICPs originated from, were smeared by 5 cm as a Gaussian. Hiro then shoot all particles in IPCs to an array consisting of 11 $\times$ 11 BaF_2 crystals. He then used a full GEANT simulation to deposit energies in BaF_2 crystals. An effective cut on minor of fitted oval, keeping more than 90% of real photons, was found to be consistent to $\bar{\theta} > 5$ mrad. Although the calculation was done for BaF_2 simulation, the same strategy can also be used for any fine segmented EMC, such as liquid argon accordion calorimeter.

Assuming that IPCs with $\bar{\theta} > 1$ mrad would be rejected by a preradiator, we can also estimate the corresponding background cross-sections after a preradiator cut. Several preradiator designs were proposed for GEM. See [6] for the details of a preradiator design for BaF_2.

As seen from Figure 7, there are single photons in IPCs which are originated from QED process in parton shower. These single photons would provide a bottom line QCD jets background for $H \rightarrow \gamma\gamma$.

Table 7 summarises the result of the QCD background cross-sections as a function of the size of the isolation cone (R) and the E_T^{cut}. The cross-sections are calculated in a $\gamma\gamma$ mass range between 75 and 165 GeV.

It is clear that a tighter isolation cut (large isolation cone and lower threshold) would provide more effective rejection, However, if R is too large or the threshold is too low, the signal acceptance would be hurt. The values applicable in analysis depends on detector performance, especially the sum of thermal and pile-up noise in a large cone.

Table 7: QCD Background Cross-Sections (pb)

After Isolation						
Process	2jets			γ-jet		
E_T^{cut}	R=0.45	R=0.60	R=0.75	R=0.45	R=0.60	R=0.75
5 GeV	140	81	46	55	45	33
10 GeV	370	220	180	100	90	76
15 GeV	780	510	360	140	120	110
20 GeV	1200	940	800	190	160	150
After Shower Shape Analysis						
Process	2jets			γ-jet		
E_T^{cut}	R=0.45	R=0.60	R=0.75	R=0.45	R=0.60	R=0.75
5 GeV	73	34	20	31	26	21
10 GeV	160	120	89	54	50	42
15 GeV	250	210	140	68	59	57
20 GeV	310	260	230	83	73	66
After Preradiator						
Process	2jets			γ-jet		
E_T^{cut}	R=0.45	R=0.60	R=0.75	R=0.45	R=0.60	R=0.75
5 GeV	20	16	13	19	17	17
10 GeV	25	20	13	24	24	19
15 GeV	34	29	20	24	24	24
20 GeV	34	34	29	26	26	26
Bottom Line QCD Background						
Process	2jets			γ-jet		
E_T^{cut}	R=0.45	R=0.60	R=0.75	R=0.45	R=0.60	R=0.75
5 GeV	10	10	7.3	17	14	14
10 GeV	13	10	7.3	19	14	14
15 GeV	16	16	13	21	17	17
20 GeV	16	16	16	21	19	17

It should also be noticed that the study carried out in this report is a straightforward one. One may try more sophisticated isolation algorithms, e.g. using central tracker or part of calorimeter etc., to relax the requirements to the calorimeter noise. We discuss briefly two algorithms of this sort which use full calorimeter information.

An algorithm summing only cells in isolation cone with energy deposition larger than three σ of noise was tested by author. Although less sensitive to the noise, this technique was found to provide a similar result to what presented in this report with some improvement. It is understood that when raising the energy threshold in each cell, the sensitivity to the associate jet energies in the isolation cone is also degraded. Another algorithm proposed by H. Ma [7] sums transverse energies in two cones with different size, both centerred at IPC, and uses different E_T^{cut} threshold in these two cones. The result of this algorithm also improves rejection efficiency.

Assuming these improved algorithms are used, the corresponding E_T^{cut} threshold in a large cone can be lowered to 2.5 times the total noise without affect the acceptance of signals.

4 H$\rightarrow \gamma\gamma$ for two GEM Calorimeter Systems

As discussed in previous section, the sum of thermal and pile-up noise in an isolation cone would affect the implementation of a tight isolation cut. The application of the isolation cut for two calorimeter systems proposed by GEM collaboration is described below.

- BaF_2 followed by a scintillation calorimeter:

  Since both BaF_2 and scintillation calorimeter have low thermal noise. The dominant contribution to the noise in a large area is the pile-up noise, which depends on integration time and luminosity. Assuming running at a standard luminosity, this system would provide around 2 GeV noise in a 0.75 isolation cone, i.e. R = 0.75 and E_T^{cut} = 5 GeV can be used.

- Liquid Argon calorimeter:

  The design of LAr system was optimised so that the thermal and pile-up noise contributions are roughly equal in a trigger tower [8]. This system has 4 GeV noise in a 0.6 isolation cone, i.e. R = 0.6 and E_T^{cut} = 10 GeV can be used.

Following the above assumption, we calculate the total background cross-section from $\gamma\gamma$, γ-jet and 2jets processes by using the isolation cut, shower shape analysis and preradiator, as discussed in previous section. The bottom line QCD background

cross-section is also calculated. Table 8 lists the total background cross-sections. Also listed in the table are the background scaling factor (B.F.) which is the total background cross-section normalized to the irreducible $\gamma\gamma$ background of 31 pb for the BaF_2 calorimeter. Note, the BaF_2 and LAr have different background cross-section because of different isolation cut used. The same difference also shows up in accepted signal cross-section.

Table 8: Total Background Cross-Section (pb)

	BaF_2 System					LAr System				
Process	$\gamma\gamma$	γ-jet	2jets	Total	B.F.	$\gamma\gamma$	γ-jet	2jets	Total	B.F.
Isol.	31	33	46	110	3.5	34	90	220	344	11
S.S.	31	21	20	72	2.3	34	50	120	204	6.6
P.R.	31	17	13	61	2.0	34	24	20	78	2.5
Irr.	31	14	7.3	52	1.7	34	14	10	58	1.9

Assuming that the shape of $\gamma\gamma$ invariant mass spectra from all background sources is the same, total background spectrum may be obtained by scaling the irreducible $\gamma\gamma$ background with a factor of B.F. Figure 9 shows spectra of Higgs signals of 80, 100, 120 and 150 GeV superimposed on total background after shower shape analysis (a) and preradiator rejection (c) for BaF_2 calorimeter. The corresponding background subtracted spectra are shown in Figure 9b) and d). The significance of these signals in one SSCY is 3.0, 5.5, 9.7 and 9.4 after shower shape analysis and 3.3, 6.0, 11 and 10 after preradiator rejection.

The same spectra are shown in Figure 10 for the LAr option. The significance in one SSCY is 1.4, 2.6, 4.5 and 4.7 after shower shape analysis, and 2.3, 4.3, 7.3 and 7.7 after preradiator rejection.

5 $Ht\bar{t} \rightarrow \gamma\gamma\ell X$ Searches

The $Ht\bar{t} \rightarrow \ell\gamma\gamma X$ is a complementary channel can be used to cover the Higgs mass range below 140 GeV [9]. As shown in Figure 1, this process has a cross-section of an order of few fb. Various background processes have been discussed in previous publications.

However, all references did not discuss in details the consequence of QCD jet background from 16 nb $t\bar{t}$ production. With a lepton tagging, the $t\bar{t}$ final state has 4 quark jets. An 1.5×10^{-3} rejection, together with a combinatory factor of 6, would provide a rejection of an order of 10^{-5} which leads to a total background cross-section from $t\bar{t} \rightarrow \ell$+4jets of 90 fb, or 50 to 80 times higher than the $Ht\bar{t} \rightarrow \gamma\gamma\ell X$ signal.

However, the $\gamma\gamma$ invariant mass distribution obtained from IPCs from $t\bar{t}$ process was spread out, a cut on interesting mass interval between 75 and 165 GeV would reduce the background by a factor of 3. It was also found that the two photon system from signal has a large p_T than that from background. A cut on joint P_T of $\gamma\gamma$ system in an order of 50 GeV would effectively reduce background by another factor of 3. It is also interesting to note that while a larger cone helps in rejecting quark jet background, the best cone size for lepton isolation is 0.3 with high signal acceptance. The following cuts are therefore used in our $Ht\bar{t} \rightarrow \gamma\gamma\ell X$ searches:

- $|\eta_\ell| < 2.5$, $P_T^\ell > 20$ GeV, R = 0.3;
- $|\eta_\gamma| < 2.5$, $P_T^\gamma > 20$ GeV, R = 0.3, 0.45 or 0.6;
- isolation cut $\Rightarrow$ reject $t\bar{t}$:

$$\sum_{r<R} E_T - E_T^{photon} < 5GeV + 0.1E_T^{photon}$$

- P_T of di-photon > 50 GeV $\Rightarrow$ reject $t\bar{t}$;
- Shower Shape Analysis: $\bar{\theta} < 5$ mrad;
- Preradiator: $\bar{\theta} < 1$ mrad.

The $Ht\bar{t} \rightarrow \gamma\gamma\ell$ signal after these cuts is in a range of 1 to 2 fb, i.e. 10 to 20 events/SSCY, as shown in Table 1. The cross-section of the $t\bar{t}$ background, calculated by using 2.6M $t\bar{t}$ events generated on PDSF, was found be reduced to less than 6 fb for most strigent cut. Table 9 summarizes the result of the calculation.

In summary, this study indicates that the $t\bar{t}$ jet background can be reduced to an acceptable level, if cuts proposed in this report are used. Further study is needed to look at other backgrounds, such as $t\bar{t}\gamma\gamma$.

Table 9: Top Background Cross-Section (fb)

R	0.3	0.45	0.6
After Isolation	280	160	68
75 GeV< $M_{\gamma\gamma}$ <165 GeV	68	43	25
$p_T(2\gamma) > 50$ GeV	31	18	6
Shower Shape	12	6	< 6
Preradiator	12	6	< 6

6 Acknowledgement

Many useful discussions with Drs. H. Gordon, J. Gunion, A. Gurtu, D. Lissauer, H. Ma, H. Newman, T. Sjostrand and H. Yamamoto are acknowledged.

References

[1] GEM Collaboration, Letter of Intent to the SSCL, November 30, 1991.

[2] CERN Green Book, *"ECFA Workshop on LEP 200"*, Aachen, September, 1986.

[3] H. Benson and T. Sjostrand, *"A Manual to the Lund Monte Carlo for Hadronic Processes"*, PYTHIA version 5.5, June, 1991.

[4] D. Dicus and S. Willenbrock, Phys. Rev. **D37** (1988) 1801.

[5] R.Y. Zhu, Proceedings of ECFA LHC Workshop, Aachen, October 1990, Volume III p. 411.

[6] H. Yamamoto, GEM Internal note GEM-TN-9133.

[7] H. Ma, GEM Internal note.

[8] BNL Report, **BNL 52244**, Ed. B.Yu and V. Radeka.

[9] W.J. Marciano and F. Paige, BNL Preprint, **BNL-45805**
J.F. Gunion *et al.*, SDC report, **SDC-91-00057**
R. Kleiss *et al.*, Phys. Let. **B253** (1991) 269;
Z. Kunszt *et al.*, Phys. Let. **B271** (1991) 247.

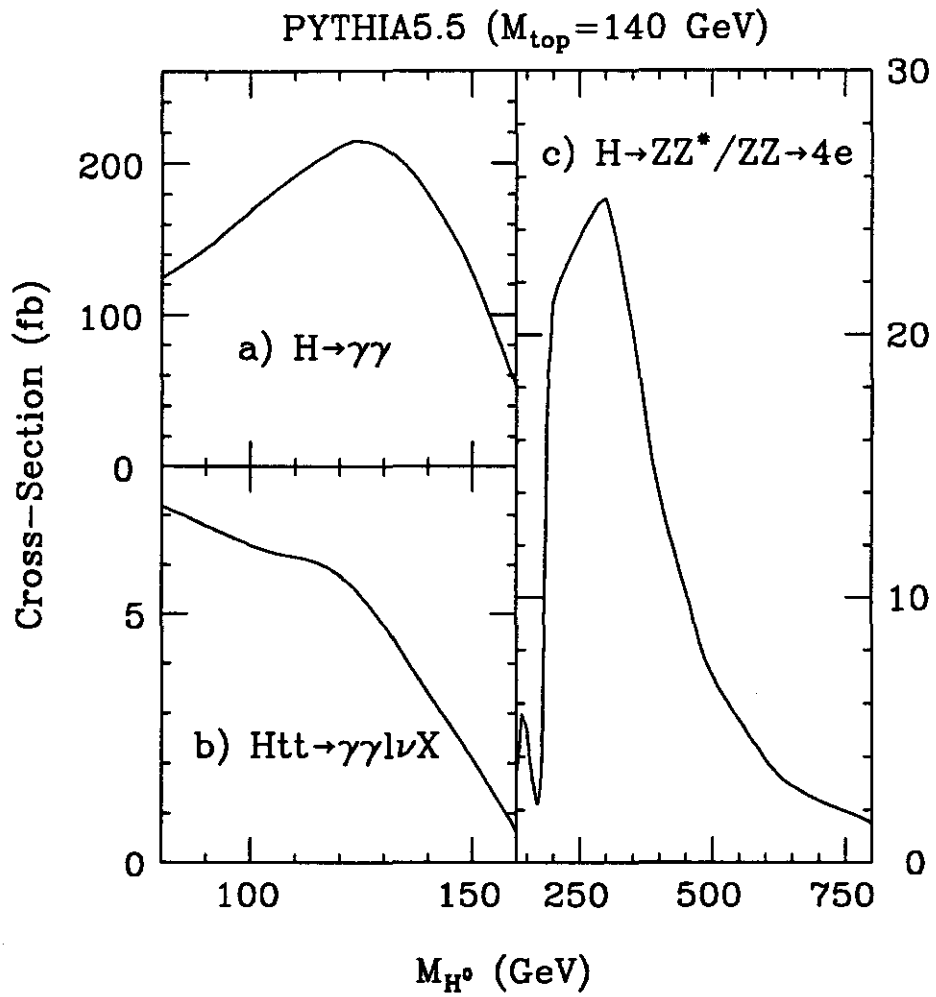

Figure 1: Cross-sections of $H^0 \rightarrow \gamma\gamma$ (a), $Ht\bar{t} \rightarrow \ell\gamma\gamma$ (b) and $H^0 \rightarrow ZZ^*/ZZ \rightarrow e^+e^-e^+e^-$ (c) events at the SSC are shown as functions of Higgs mass.

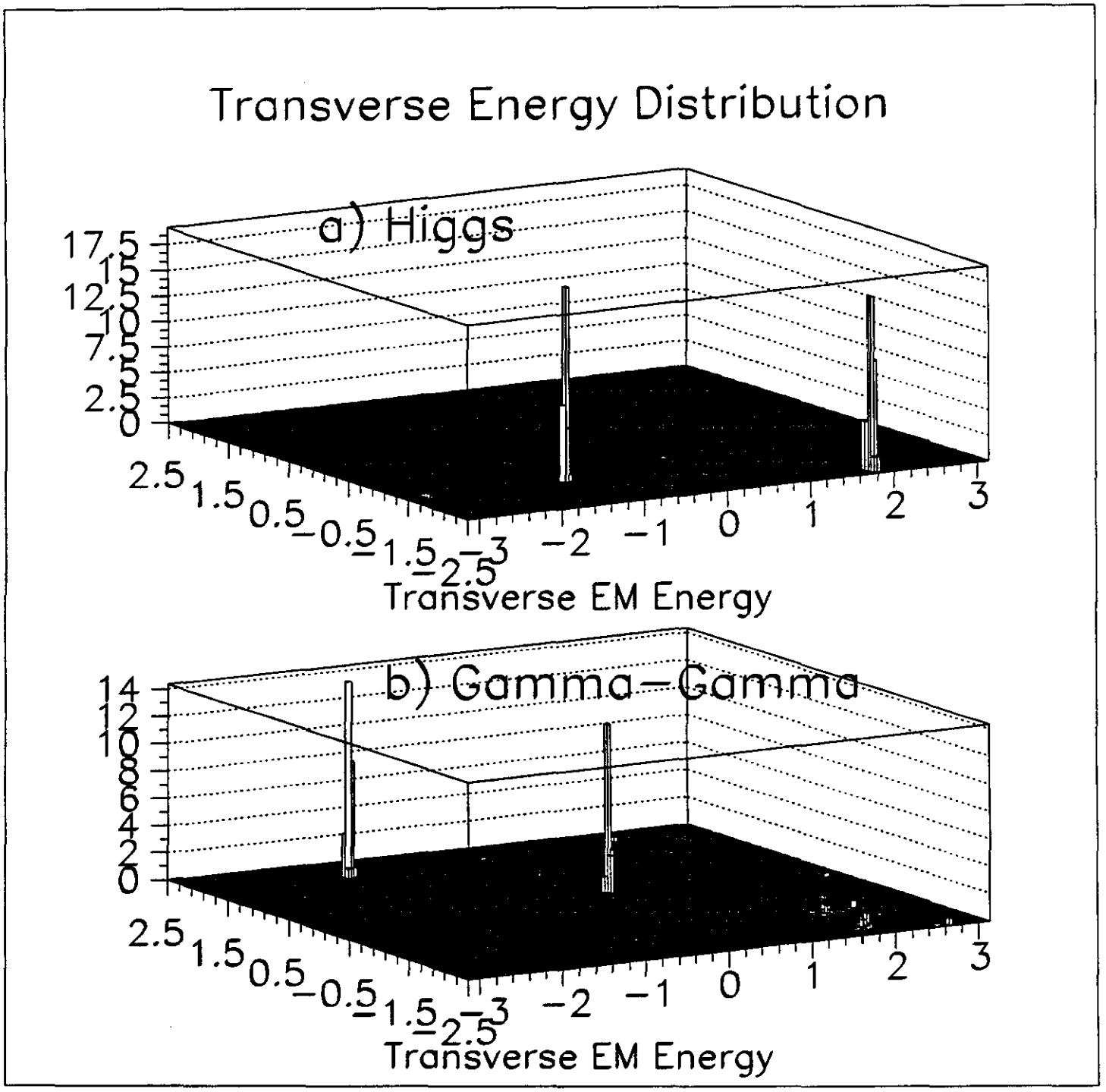

Figure 2: Transverse energy distributions in EMC for two typical events from signal process of H→ $\gamma\gamma$ (a) and irreducible background process $\gamma\gamma$ (b).

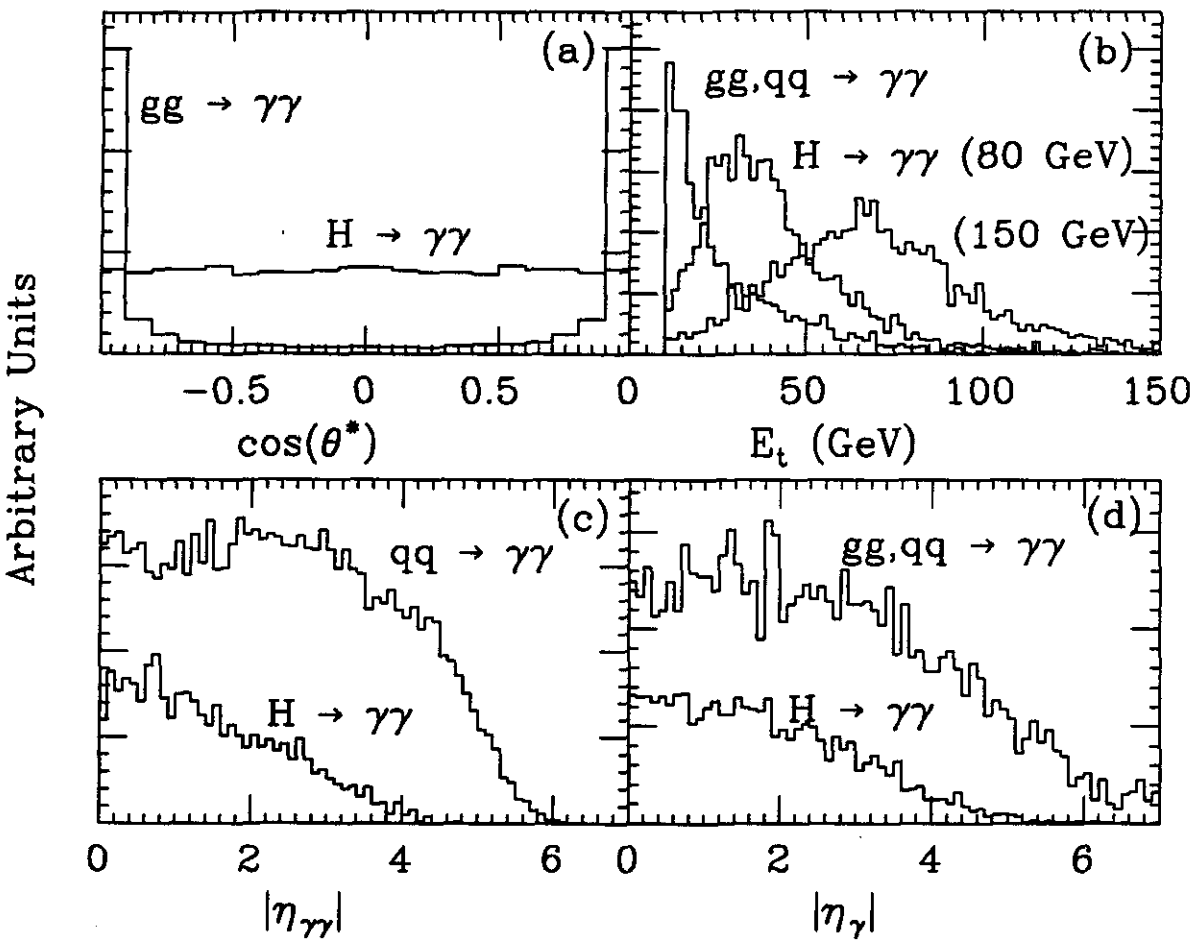

Figure 3: Distributions of a) $\cos\theta^*_\gamma$, b) E^γ_T, c) $|\eta_{\gamma\gamma}|$; and d) $|\eta_\gamma|$.

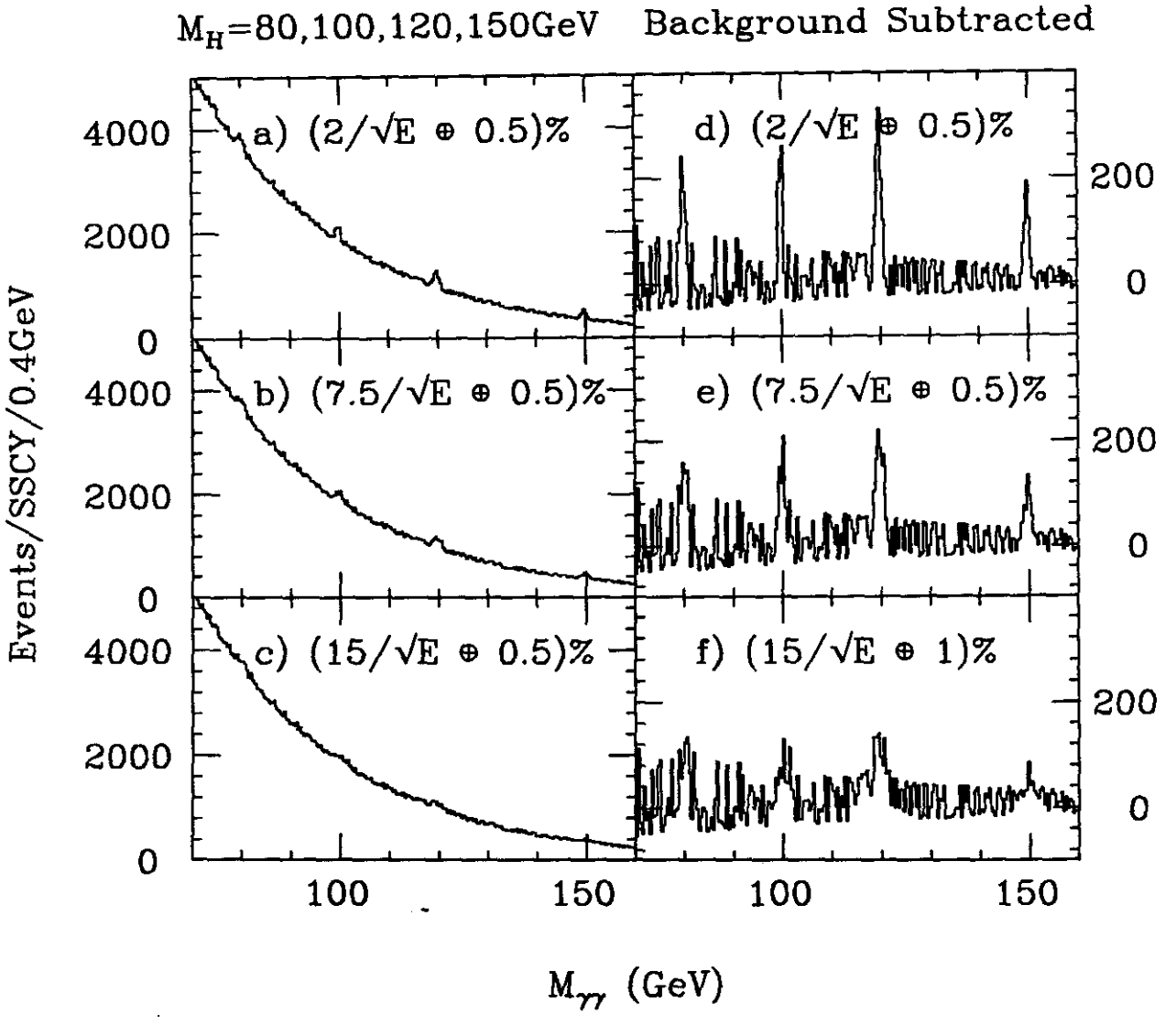

Figure 4: $\gamma\gamma$ invariant mass spectra obtained within 1 SSCY with H$\rightarrow$ $\gamma\gamma$ signals of 80, 100, 120 and 150 GeV, superimposed on irreduciable background are shown for three energy resolutions: a) $(2/\sqrt{E} \oplus 0.5)\%$; b) $(7.5/\sqrt{E} \oplus 0.5)\%$; and c) $(15/\sqrt{E} \oplus 1.0)\%$. Corresponding background subtracted spectra are shown in d), e) and f).

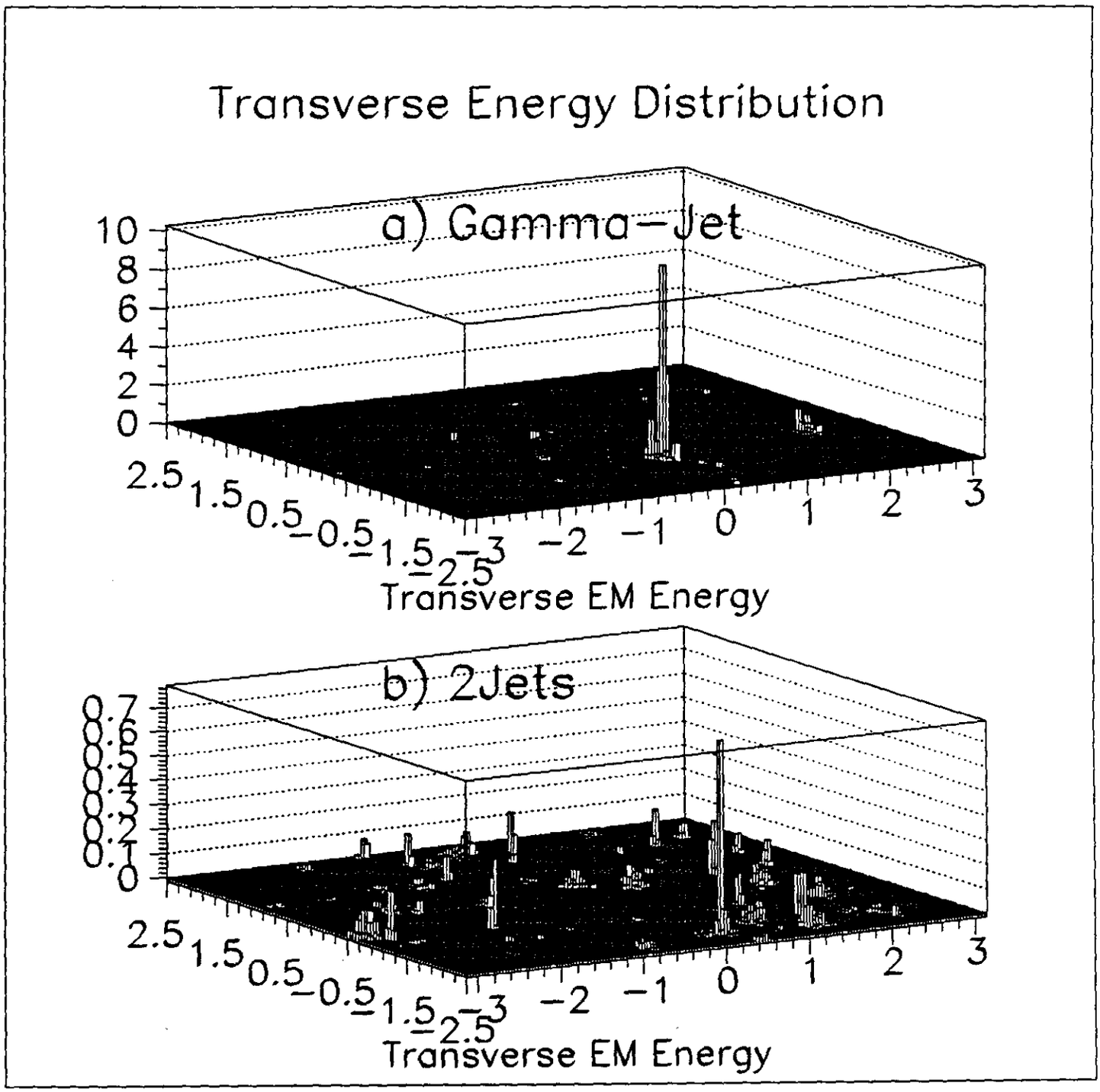

Figure 5: Transverse energy distributions in EMC for two typical events from background processes: (a) γ-jet and (b) 2jets.

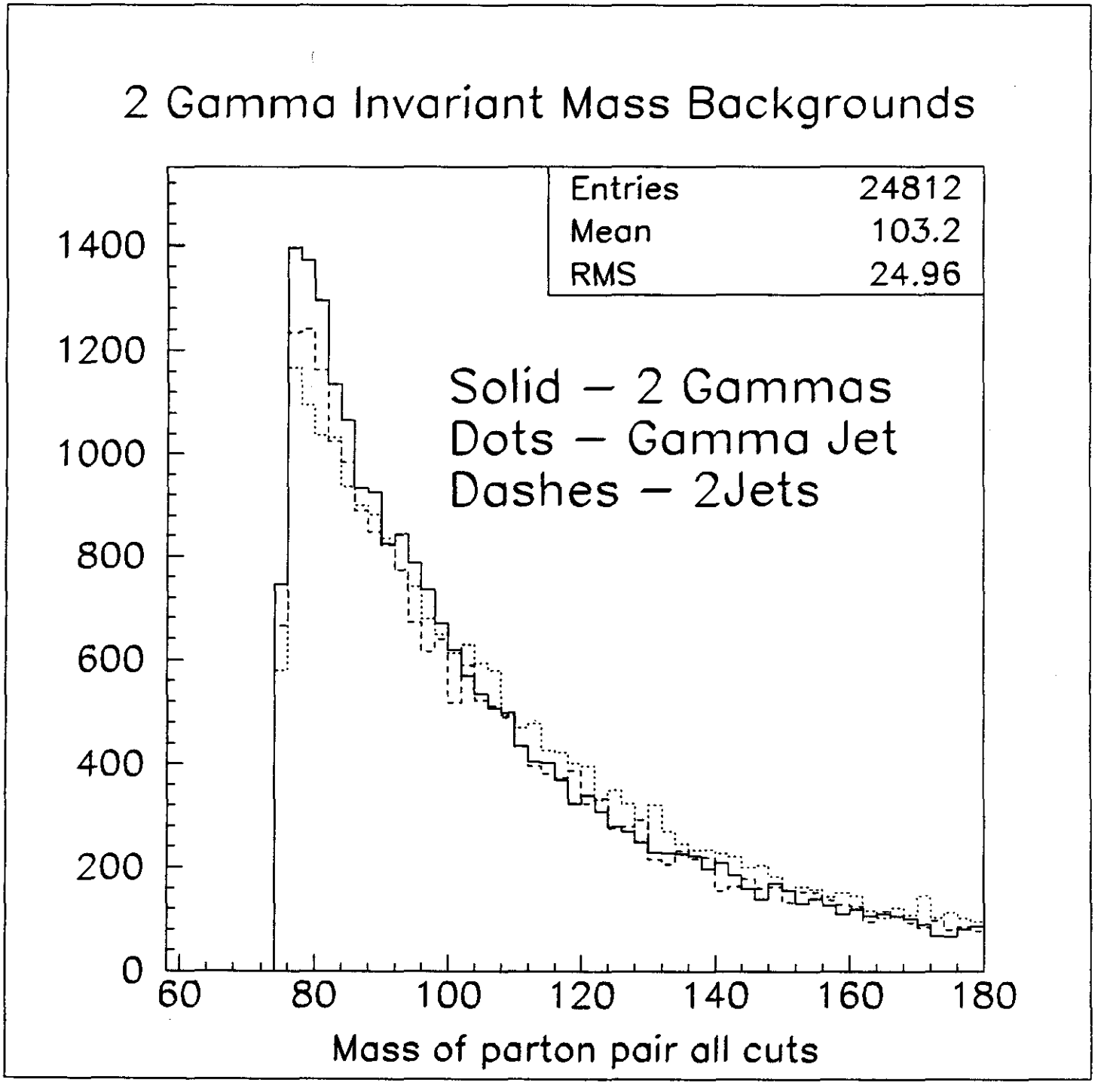

Figure 6: Comparison of parton invariant mass spectra from three QCD processes: $\gamma\gamma$, γ-jet and 2jets.

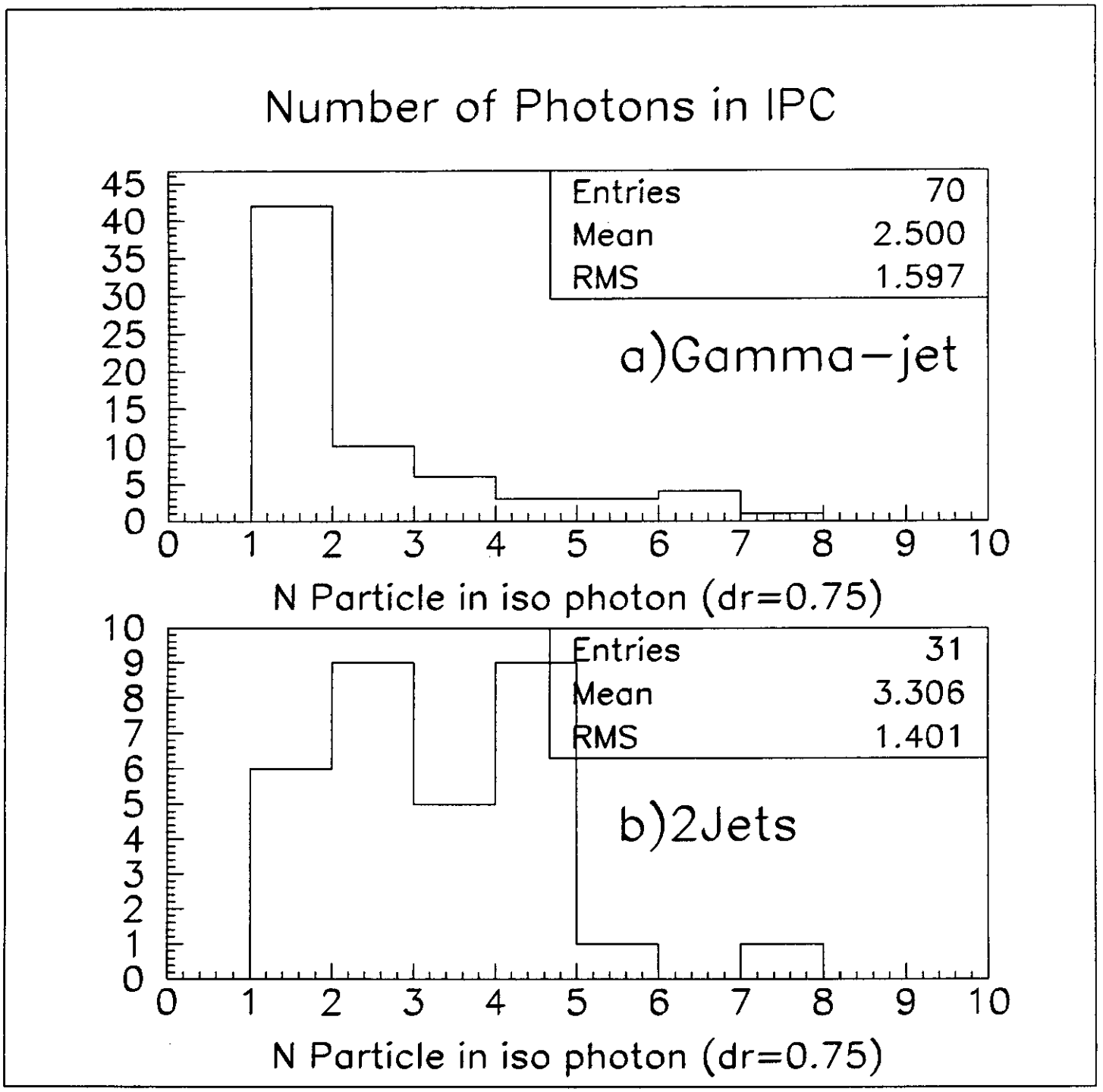

Figure 7: Distributions of photon numbers in isolated photon candidates, passing an isolation cut of R = 0.75 and E_T^{cut} = 10 GeV from 100k events each of (a) γ-jet and (b) 2jets.

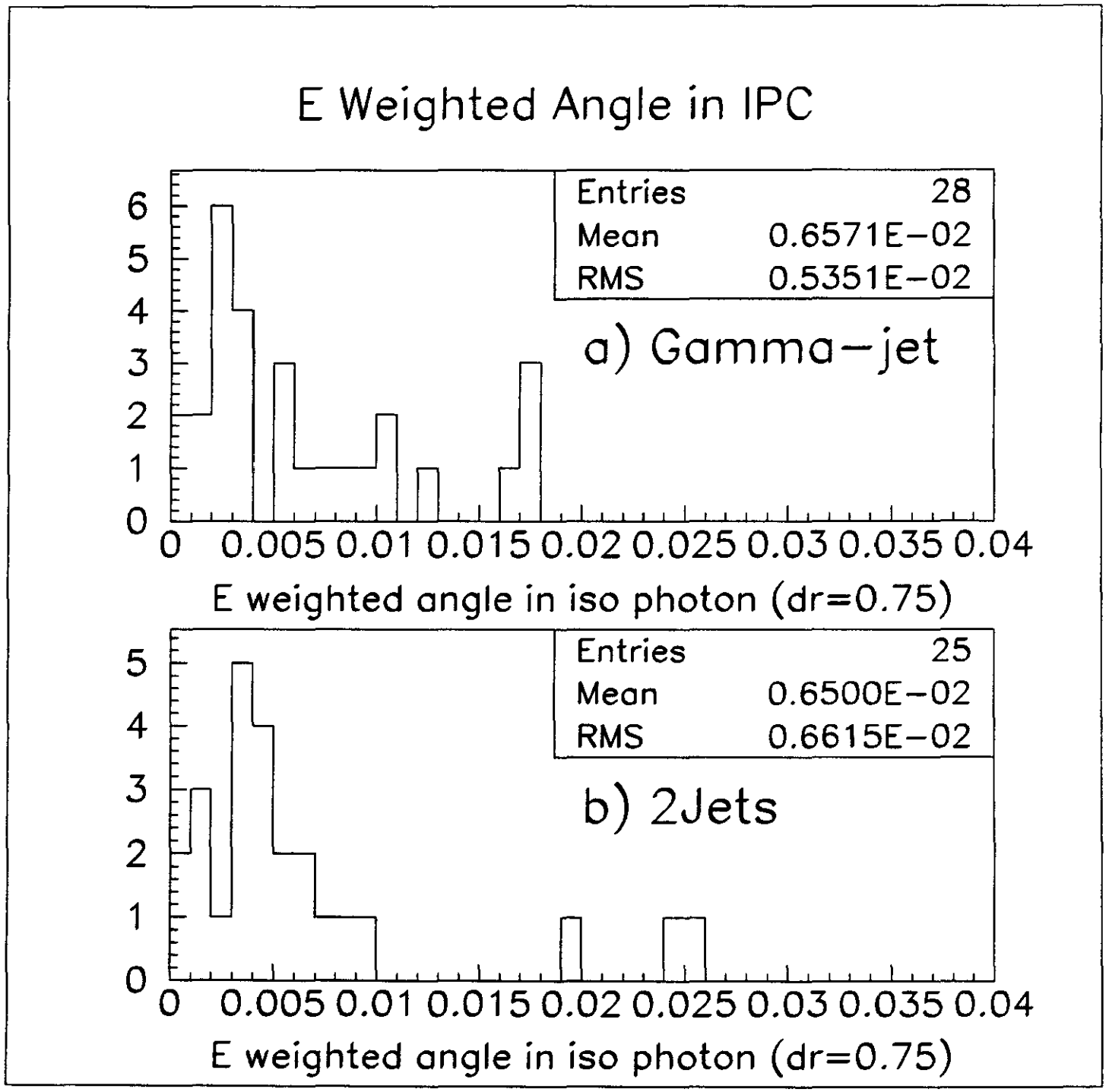

Figure 8: Distributions of $\bar{\theta}$ ofisolated photon candidates, passing an isolation cut of R = 0.75 and E_T^{cut} = 10 GeV from 100k events each of (a) γ-jet and (b) 2jets.

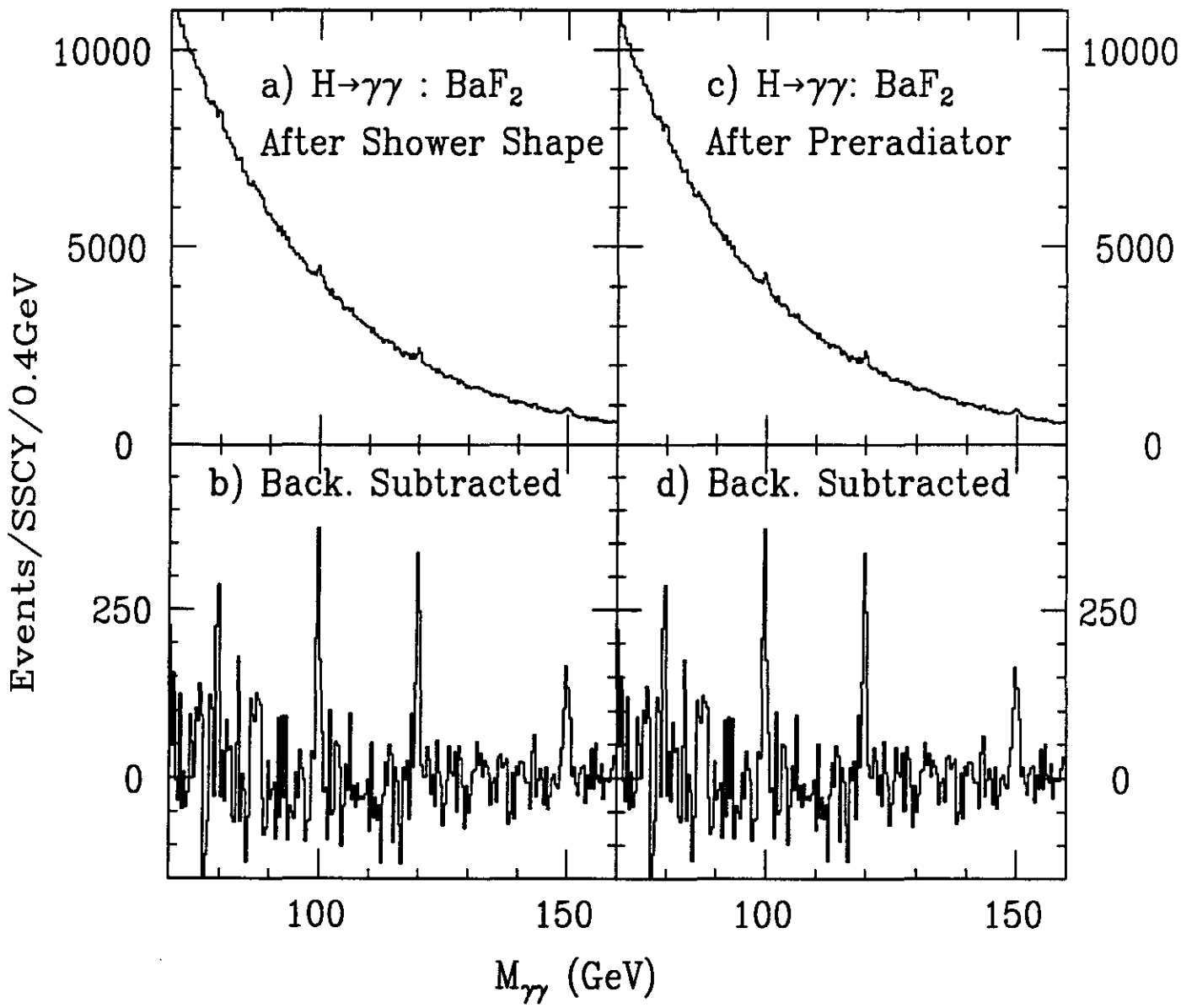

Figure 9: H→ $\gamma\gamma$ signals of 80, 100, 120 and 150 GeV, superimposed on all backgrounds are shown for BaF_2 calorimeter after shower shape analysis (a) and preradiator rejection (c). Corresponding background subtracted spectra are shown in (b) and (d).

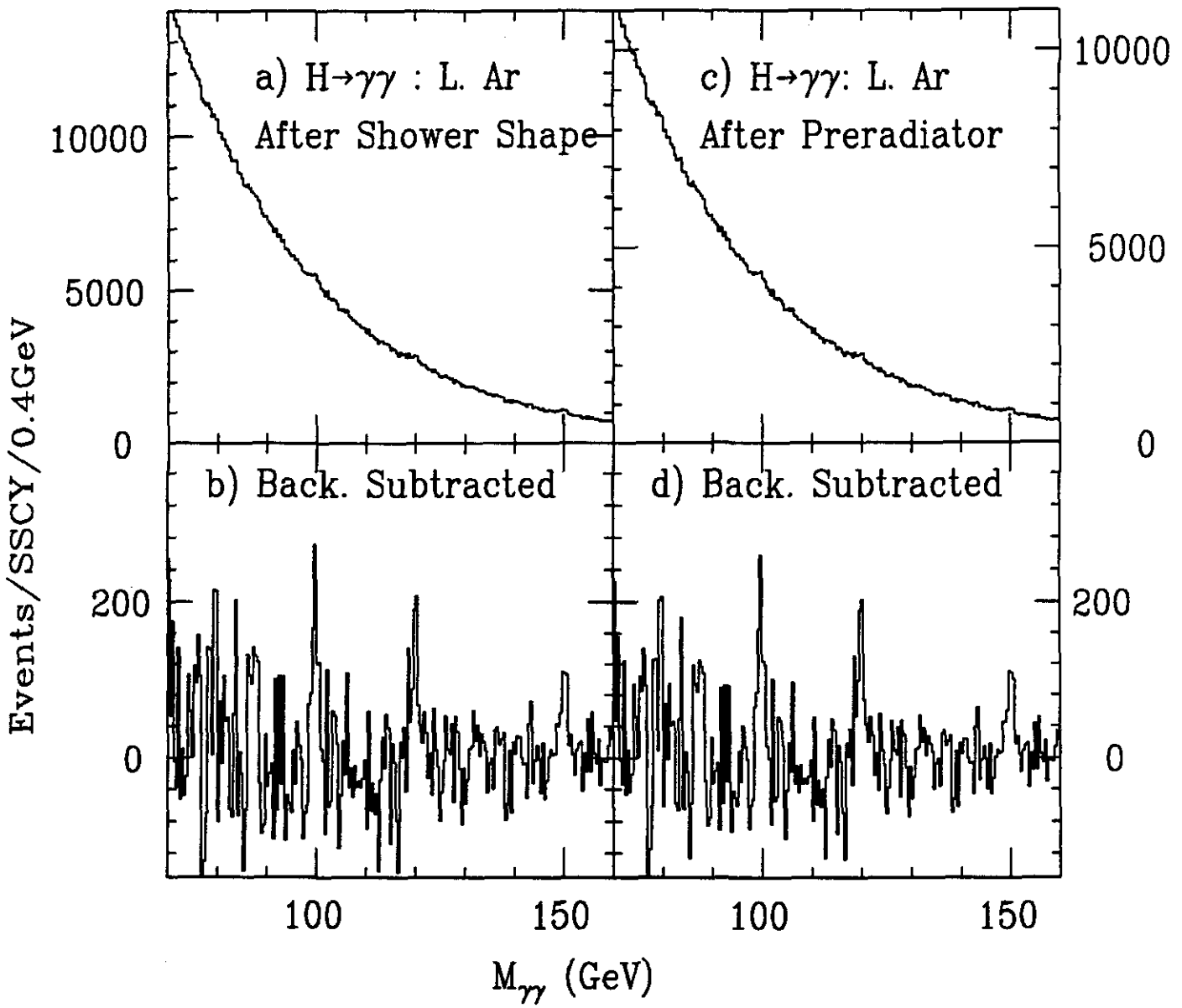

Figure 10: H→ $\gamma\gamma$ signals of 80, 100, 120 and 150 GeV, superimposed on all backgrounds are shown for LAr calorimeter after shower shape analysis (a) and preradiator rejection (c). Corresponding background subtracted spectra are shown in (b) and (d).